Optically injected quantum-dot lasers

T. Erneux,[1] E. A. Viktorov,[1] B. Kelleher,[2,3,*] D. Goulding,[2,3] S. P. Hegarty,[2,3] and G. Huyet[2,3]

[1]*Université Libre de Bruxelles, Optique Nonlinéaire Théorique, Campus Plaine, Code Postal 231, 1050 Bruxelles, Belgium*
[2]*Tyndall National Institute, Lee Maltings, Cork, Ireland*
[3]*Department of Applied Physics and Instrumentation, Cork Institute of Technology, Cork, Ireland*
**Corresponding author: bryan.kelleher@tyndall.ie*

Received July 22, 2009; revised February 3, 2010; accepted February 4, 2010;
posted February 25, 2010 (Doc. ID 114600); published March 19, 2010

The response of an optically injected quantum-dot semiconductor laser (SL) is studied both experimentally and theoretically. In particular, the nature of the locking boundaries is investigated, revealing features more commonly associated with Class A lasers rather than conventional Class B SLs. Experimentally, two features stand out; the first is an absence of instabilities resulting from relaxation oscillations, and the second is the observation of a region of bistability between two locked solutions. Using rate equations appropriate for quantum-dot lasers, we analytically determine the stability diagram in terms of the injection rate and frequency detuning. Of particular interest are the Hopf and saddle-node locking boundaries that explain how the experimentally observed phenomena appear. © 2010 Optical Society of America

OCIS codes: 030.1640, 140.3490, 140.3520, 140.5960, 250.5590.

Typically, when a laser is perturbed from its steady-state operation, it either approaches the equilibrium exponentially like an overdamped oscillator or slowly oscillates back to its stable steady state like an underdamped oscillator. These lasers are labeled as Class A and Class B, respectively. Class A lasers include Ar, He–Ne, and dye lasers, while Class B lasers include most of the lasers used today such as CO_2, solid-state, and, most importantly for this work, semiconductor lasers (SLs). When subject to optical injection, Class A and Class B lasers exhibit quite different stability properties. Class B lasers admit a rich number of sustained pulsating intensity regimes related to their relaxation oscillations (ROs), which have been studied systematically over the past decade for semiconductor and solid-state lasers (see [1] for a recent review). Class A lasers, free of ROs, are much more stable [2]. Recent efforts have concentrated on increasing the photon lifetime above the carrier lifetime to suppress ROs in conventional SLs. This can be achieved by increasing either the cavity length or the cavity finesse [3,4].

In this Letter we consider both experimentally and theoretically the optical injection of a single-mode distributed feedback (DFB) quantum-dot laser (QDL). These lasers have been increasingly investigated in recent years, and studies have already revealed several dynamical properties that render them superior for applications [5]. A particular feature of these devices is an unusually high damping of the ROs [6,7] in comparison with their bulk and quantum well (QW) counterparts. This high damping has been cited as the principal reason for the increased stability of such devices when subject to optical feedback [8], optical injection [9], and in mutual coupling [10] configurations. We determine an experimental stability diagram and note that it is considerably different to that of a conventional QW laser. In particular, there is an absence of RO-related phenomena, and there is a region of bistability between two coexisting fixed points. Although these features were noted in [9], in this Letter we examine the result in greater depth, and the observations are substantiated analytically by studying rate equations appropriate for a QDL.

The QDLs used were DFB structures operating at a wavelength of approximately 1.3 μm. The experimental setup is similar to the one described in [11]. The results of the experimental stability mapping are shown in Fig. 1. The solid (black) lines are saddle-node (SN) bifurcations, and the dashed (red) lines are Hopf bifurcations. Various dynamical features were observed, but the one of most interest for this work is the domain of bistable operation, in which two locked steady states coexist and the laser displays a noise-induced switching, as shown in the inset of Fig. 1. There are a number of fundamental differences between the mapping in Fig. 1 and the injection dynamics reported in [12] for a conventional QW laser and reviewed in detail in [1]. The Hopf bifurcation line differs from that which occurs for an injected QW la-

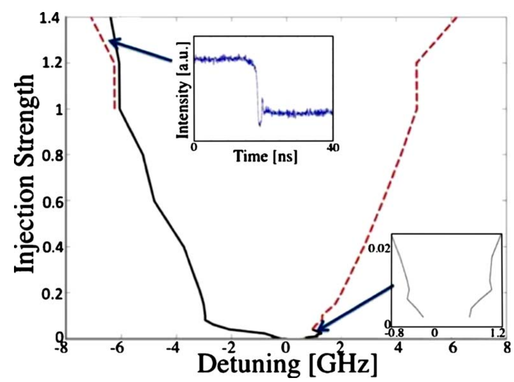

Fig. 1. (Color online) Experimental stability diagram. The solid (black) lines are saddle-node bifurcations, while the dashed (red) lines are Hopf bifurcations. The injection strength is defined as the power of the light injected into the cavity divided by the power in the cavity when free running. One inset shows switching between two locked states with different intensities; the other inset shows a zoom of the region of low injection strength where the locking is via a saddle-node bifurcation for both signs of the detuning.

0146-9592/10/070937-3/$15.00

ser and, in particular, it does not cross the zero detuning line. Furthermore, except very close to the laser threshold [13], the coexistence of two stable locking states is not possible for an optically injected QW laser. Instead, we note a similarity between the stability diagram in Fig. 1 and that of a Class A laser [2]. More precisely, QDLs may exhibit both Class A and Class B dynamics, depending on the carrier capture parameters as was shown in [7] by analyzing a three-variable rate-equation model. In this Letter, we consider these equations for the case of an optically injected laser and examine the limit that leads to the highest damping of the ROs.

Our rate equations for a QD laser subject to an injected signal consist of three equations for the complex electric field E, the occupation probability in a dot ρ, and the carrier density n in the wetting layers, scaled to the 2D QD density per layer. Adding the injection term to the rate equations of the solitary laser [7], we find

$$E' = \frac{1}{2}(1+i\alpha)[-1+g(2\rho-1)]E + \Gamma \exp(i\Delta t), \quad (1)$$

$$\rho' = \eta[Bn(1-\rho) - \rho - (2\rho-1)|E|^2], \quad (2)$$

$$n' = \eta[J - n - 2Bn(1-\rho)]. \quad (3)$$

The prime means differentiation with respect to $T \equiv t/\tau_{ph}$, where t is time and τ_{ph} is the photon lifetime. The factor 2 in Eq. (3) accounts for the spin degeneracy in the QD energy levels. J is the pump current per dot, and α is the linewidth enhancement factor. The control parameters are the frequency detuning Δ defined as the frequency of the master laser minus that of the slave laser and the injection rate Γ. The fixed parameters B and η are ratios of basic time scales and are defined as $B \equiv \tau\tau_{cap}^{-1}$ and $\eta \equiv \tau_{ph}\tau^{-1}$, where τ and τ_{cap} denote the carrier recombination and capture times, respectively. Typical values are $\tau = 1$ ns and $\tau_{cap} = 10$ ps, which imply $B = 10^2$ and $\eta = 2 \times 10^{-3}$. The factor $(1-\rho)$ is the Pauli blocking factor. The nonlinear interaction between the wetting layer and the dot, provided by the Pauli blocking factor, is nonnegligible and constitutes the most important difference between the description of QDLs and that of more conventional semiconductor devices.

As suggested in [9], we shall consider the value $g = 1.01$, for which a good agreement between theory and experiments is observed. In the case of the solitary laser ($\Gamma = 0$), the product $B(g-1)$ appears in both the steady-state expressions and in the characteristic equation [7]. Therefore we need to take into account the relative values of B and $g-1$. Specifically, we propose an asymptotic analysis of Eqs. (1)–(3) valid in the limit of small $\epsilon \equiv g-1$, keeping $B\epsilon$ as an $O(1)$ quantity. After introducing $g = 1+\epsilon$ into Eq. (1), the expression in brackets becomes $[-2+2\rho+\epsilon(2\rho-1)]$ and suggests the introduction of $\rho = 1+\epsilon u$ in order to balance all terms. The expression in brackets is then proportional to ϵ, which motivates the introduction of the slow time scale $s \equiv \epsilon T$. From Eqs. (1)–(3), we obtain the following equations for E, u, and n:

$$E' = \frac{1}{2}(1+i\alpha)[1+2u(1+\epsilon)]E + \gamma \exp(i\delta s), \quad (4)$$

$$u' = \epsilon^{-2}\eta[-B\epsilon nu - 1 - \epsilon u - (1+2u\epsilon)|E|^2], \quad (5)$$

$$n' = \epsilon^{-1}\eta[J - n + 2B\epsilon nu], \quad (6)$$

where the prime now means differentiation with respect to s. The control parameters are $\gamma \equiv \epsilon^{-1}\Gamma$ and $\delta \equiv \epsilon^{-1}\Delta$. Since $\epsilon^{-2} \gg \epsilon^{-1}$ as $\epsilon \to 0$, we adiabatically eliminate u. Specifically, we find $u = -(1+E^2)/(B\epsilon n)$ as $\epsilon \to 0$. Introducing the decomposition $E = Re^{(i\delta s + i\phi)}$, Eqs. (4)–(6) then reduce to three equations for R, ϕ, and n. The threshold of the solitary laser appears at $J = J_{th} \equiv 2 + 2/(B\epsilon)$. Assuming $J > J_{th}$, we determine the steady-state solution $R_s^2 = R_s^2(\gamma)$ in the implicit form $\gamma = \gamma(R_s^2)$. From the three variable linearized equations, we formulate the characteristic equation

$$\lambda^3 + a_1\lambda^2 + a_2\lambda + a_3 = 0 \quad (7)$$

for the growth rate λ, where all coefficients can be expressed in terms of R_s^2 rather than γ. The Routh–Hurwitz stability conditions are $a_1a_2 - a_3 > 0$, $a_1 > 0$, and $a_3 > 0$. An SN bifurcation point satisfies the condition $a_3 = 0$; a Hopf bifurcation point satisfies the condition $a_1a_2 - a_3 = 0$. Both conditions can be solved analytically, because they are quadratic equations in the detuning δ. We first determine δ as a function of R_s^2 from the SN and Hopf conditions and then δ as a function of γ using the steady-state equation $\gamma = \gamma(R_s^2)$. The stability diagram is shown in Fig. 2. Only the Hopf bifurcation points from a stable steady state are shown ($a_1a_2 - a_3 = 0$, $a_1 > 0$, and $a_3 > 0$) for clarity.

The stability diagram in Fig. 2 is qualitatively similar to the experimental mapping. Both the ex-

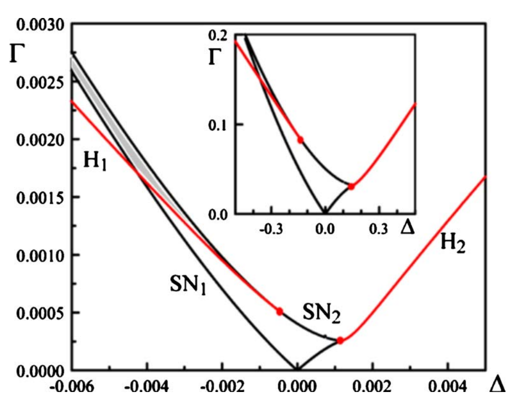

Fig. 2. (Color online) Analytic stability diagram. SN and H denote the saddle-node and Hopf bifurcation points, respectively. The shaded region corresponds to the domain of steady-state bistability. The values of the parameters are $g = 1.01$, $B = 10^2$, $\eta = 2 \times 10^{-3}$, $\alpha = 1.2$, and $J = 1.2J_{th} = 4.8$ ($J_{th} = 4$). The dots are fold-Hopf points where Hopf and SN bifurcation lines merge. Inset, stability diagram for an injected Class A laser (Eq. (1) in [2] with $\Gamma\kappa^{-1} = 1.2$, $\alpha = 1.2$, $\beta = 1$, $\Gamma \to \sigma S\kappa^{-1}$, $\Delta \to -\Delta\Omega\kappa^{-1}$, and $t \to \kappa t$).

perimental and analytical stability diagrams predict stable locking for arbitrary values of the injection rate, provided $|\Delta|$ is sufficiently small. Moreover, there are no Hopf bifurcations at low injection levels, which was previously suspected in [11]. At higher injection levels and for positive detuning, the locking is via a Hopf bifurcation (H_2 in Fig. 2), and there is no SN bifurcation. For negative detunings, there is a domain of bistability between two locked states, possible here because of a Hopf bifurcation that stabilizes the lower intensity branch (H_1 in Fig. 2). Two bifurcation diagrams of the stable steady-state and periodic regimes are shown in Fig. 3. They have been determined numerically from the reduced equations for R, ϕ, and n.

Because the Hopf bifurcation curves do not cross the zero detuning line as is the case for QW SLs, the injected QDL exhibits greater stability. We should, however, emphasize that the similarity between our QD laser and the Class A laser results from the conditions $g-1 \ll 1$ and $(g-1)B = O(1)$ and is valid for $\eta \ll 1$. Other scalings of the parameters $g-1$ and B are possible because of the large diversity of QD structures that are currently designed, possibly leading to different conclusions.

In conclusion, we have performed an experimental and theoretical study of an optically injected single-mode QDL. Two principal features were obtained and discussed. First, the Hopf bifurcation associated with the ROs in Class B devices is absent in a large region of the stability diagram where the laser is stably

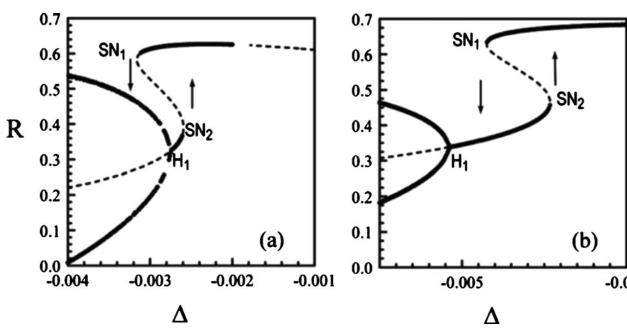

Fig. 3. Bifurcation diagrams of the stable steady-state and time-periodic solutions. The extrema of R are shown as functions of the detuning Δ. The complete S-shaped branch of steady states is shown by a broken curve. The values of the parameters are the same as in the previous figure. (a) Regions of coexistence between two locked states and coexistence between a locked state and an unlocked limit cycle both exist for $\Gamma = 0.0012$ and (b) coexistence between two locked solutions only for $\Gamma = 0.002$. The figures were obtained by scanning the detuning back and forth.

locked, suggesting that QD lasers may be of interest for applications requiring RO-free operation. Secondly, there is a region of bistability between two locked solutions. These attributes are markedly different from the case with conventional semiconductor lasers and are more characteristic of an optically injected Class A laser.

This work was conducted under the framework of the INSPIRE programme, funded by the Irish Governments Programme for Research in Third Level Institutions, Cycle 4, National Development Plan 2007–2013, and the authors also gratefully acknowledge the support of Science Foundation Ireland (SFI) under contact 07/IN.1/I929, the Irish Research Council for Science, Engineering and Technology (IRCSET), and the Tyndall National Access Programme. The authors in Bruxelles acknowledge support of the Fonds National de la Recherche Scientifique (Belgium). The research by T. E. was supported by Air Force Office of Scientific Research (AFOSR) grant FA8655-09-1-3068.

References

1. S. Wieczorek, B. Krauskopf, T. Simpson, and D. Lenstra, Phys. Rep. **416**, 1 (2005).
2. C. Mayol, R. Toral, C. R. Mirasso, and M. A. Natiello, Phys. Rev. A **66**, 013808 (2002).
3. G. Baili, M. Alouini, C. Moronvalle, D. Dolfi, and F. Bretenaker, Opt. Lett. **31**, 62 (2006).
4. G. Baili, M. Alouini, T. Malherbe, D. Dolfi, I. Sagnes, and F. Bretanker, Europhys. Lett. **87**, 44005 (2009).
5. D. Bimberg, M. Grundmann, and N. N. Ledentsov, *Quantum Dot Heterostructures* (Wiley, 1999).
6. K. Lüdge, M. J. P. Bormann, E. Malic, P. Hövel, M. Kuntz, D. Bimberg, A. Knorr, and E. Schöll, Phys. Rev. B **78**, 035316 (2008).
7. T. Erneux, E. A. Viktorov, and P. Mandel, Phys. Rev. A **76**, 023819 (2007).
8. D. O'Brien, S. P. Hegarty, G. Huyet, and A. V. Uskov, Opt. Lett. **29**, 1072 (2004).
9. D. Goulding, S. P. Hegarty, O. Rasskazov, S. Melnik, M. Hartnett, G. Greene, J. G. McInerney, D. Rachinskii, and G. Huyet, Phys. Rev. Lett. **98**, 153903 (2007).
10. S. P. Hegarty, D. Goulding, B. Kelleher, G. Huyet, M. T. Todaro, A. Salhi, A. Passaseo, and M. De Vittorio, Opt. Lett. **32**, 3245 (2007).
11. B. Kelleher, D. Goulding, S. P. Hegarty, G. Huyet, Ding-Yi Cong, A. Martinez, A. Lemaître, A. Ramdane, M. Fischer, F. Gerschütz, and J. Koeth, Opt. Lett. **34**, 40 (2009).
12. T. B. Simpson, Opt. Commun. **215**, 135 (2003).
13. A. Hohl, H. J. C. van der Linden, R. Roy, G. Goldsztein, F. Broner, and S. H. Strogatz, Phys. Rev. Lett. **74**, 2220 (1995).